# Intercomparison of Local and Non-Local Atmospheric Boundary-Layer Schemes in *MM5* with Detailed Observations

[FINAL DRAFT]

Olaf S. Vellinga
Meteorology and Air Quality Group, Wageningen University, The Netherlands

Short title:

**Abstract.** Within the context of air-quality research, the development and maintenance of a convective boundary-layer (CBL) during two days is studied by means of a mesoscale weather-forecast model *MM5* and detailed surface and upper-air observations. Model results for four different boundary-layer schemes, grouped in categories of local and non-local parameterizations, are compared to the observations. Because output-data of mesoscale models are more often used as input-data for air-quality models to determine the mixing-layer depths, this study concentrated on parameters that are crucial to the day-time mixing-layer development. It was found that for the surface fluxes, all schemes overestimate largely both heat fluxes, which is related to the overestimations of the friction velocity, the wind-speed, and the temperature difference and the moisture difference between the ground and the surface layer. Here, the local schemes agree better with the observations than the non-local schemes. For the vertical profiles, on both days all schemes show colder and more humid CBLs with underestimated inversions than the observations, which is a contradictory result regarding the large overestimations of both heat fluxes. The non-local schemes capture better the vertical structure and show lower biases than the local schemes. For the mixing-layer height, all schemes underestimate the observed depths for both days. However, the non-local schemes agree better with the observations than the local schemes. Results of the second day show larger disagreements with the measurements due to possible non-local synoptic effects that were not correctly captured by the model. It is, therefore, recommended for air-quality modelling to use non-local schemes in *MM5* for mixing-layer depth predictions.

## 1. Introduction [final draft]

Mesoscale weather-forecast models are currently used to simulate and to forecast short-range meteorological and air-pollution situations. Output-data of these 3D numerical models are increasingly being used as a key-input for air-quality models (AQMs), as meteorological data are required for performing the necessary tasks, *i.e.*, forecasting the transport, dispersion and removal of air-pollutants. Todays state-of-science meteorological models have still difficulties to perform reasonable on meso-$\beta$-scale or smaller, as has been stated by *Hogrefe et al.* [2001]. However, as they are mainly the only consistent data-source on time and space with regard to meteorological fields, they have become widely accepted for air-quality applications. Fortunately, they are improving with rapid speed as computers get more powerful, new data-sources — like remote sensing technologies — get available, and additional techniques — like non-hydrostatic mathematical frameworks and four dimensional data assimilation techniques — are incorporated into these models [*Seaman*, 2000]. Despite of this positive fact, most research on improving those models is still being done by testing them on large synoptic scale phenomena, like hurricanes or frontal zones. Within the context of air-quality studies, on the other hand, weak synoptic forcing during summer day-time periods are a more important subject to research, for instance the development and evolution of a convective boundary layer (CBL). Especially, CBLs in which cumulus-convection is absent are necessary to study in detail, because air-pollutants are trapped within this layer. Consequently, the concentration of those pollutants will be influenced, among others, by the depth of the PBL. Therefore, if the depth is not correctly determined, errors will occur in the value of the concentrations. As output-data from mesoscale models used for determining the day-time mixing-layer depth frequently contain inaccuracies [*Seaman*, 2000; *Hogrefe et al.*, 2001], the forecasted concentrations of air-pollutants may often be erroneous. This may result in faulty predictions of degradation of air-quality in certain regions. This is the reason why validation is needed to improve weather-forecast models to produce more accurate data on weakly forced circulations, mixing-layer depths and turbulent mixing-processes. By doing this, more insight into the deficiencies of mesoscale models could increase the ability of these models to represent the main characteristics and variables in the ABL more realistic for the relevant length and time scales.

A mesoscale models widely used for AQMs applications is the non-hydrostatic *Fifth-Generation* PSU/NCAR *Mesoscale Model* (*MM5*) from the Pennsylvania-State University and the U.S. National Center of Atmospheric Research [*Grell et al.*, 1995]. It has become common practice to use it as one of the meteorological pre-processors for AQMs [*Seaman*, 2000; *Hogrefe et al.*, 2001]. Therefore, it is relevant to study more closely the physics incorporated into the model with regard to air-quality

studies. For this matter, the parameterizations for describing the surface fluxes and boundary-layer processes implemented into the *MM5* modelling-system are of main interest. The boundary-layer parameterizations in the model, which can be selected, can be classified into two groups: a group based upon non-local closure theory; and a group based upon local closure theory. To the first group belong, for instance, the PBL-schemes developed by *Blackadar* [1976], called *High-Resolution Blackadar* (hereafter referred to as BLA); and the one of *Hong and Pan* [1996] that is also known as the *Medium-Range Forecast* parameterization (hereafter referred to as MRF). This group concentrates on surface and bulk layer variables, where the vertical mixing is realized between non-adjacent layers. The second group contains higher-order, local closure schemes, in which the turbulent fluxes are a function of the turbulent kinetic energy. Some of the latter type of parameterizations are — among others — the PBL-scheme as it is implemented in the *Eta-model* of the U.S. National Center for Environmental Prediction (NCEP) [*Janjić*, 1990] using a Mellor-Yamada scheme (hereafter referred to as Eta); and the one developed by *Burk and Thompson* [1989] additionally using their version of the Mellor-Yamada scheme (hereafter referred to as BRT). In this current study, all four parameterizations, mentioned here, are being investigated.

Regarding this area of model research, previous studies (*Seaman et al.* [1989]; *Berman and Rao* [1999]; *Braun and Tao* [2000]) have already investigated whether *MM5* was able to successfully simulate the main ABL-processes and its evolution. However, these boundary-layer studies occurred under meteorological situations with a high degree of complexity: urban area, coastal zone, ABL in a hurricane. Moreover, the observational validation was not as complete as in this current study. *Zamora et al.* [2000] also studied the evolution of a CBL at Nashville by using *MM5*. However, they did not perform a sensitivity analysis of the various boundary-layer representations available in the modelling-system. This current study is an extension of the previous studies and is focused on critically evaluating the performance of two days at surface and upper air-levels of the PBL-descriptions compared to a complete, detailed set of field measurements from, respectively, the observational tower at Cabauw, The Netherlands, and the *Royal Dutch Meteorological Institute* (KNMI) in De Bilt, The Netherlands.

Hence, the contributions of this paper — within the context of air-quality modelling — can be summarized as follows: 1.) simulating a clear convective case with the atmospheric boundary-layer schemes as they are available in the version of *MM5* used in this study; 2.) analyzing the representiveness of each scheme by comparison to field observations with emphasis on parameters that are most crucial to the mixing-layer depth developments; 3.) to create conclusions on the schemes' general performance for the clear convective case with regard to reproducing correct day-time mixing-layer depths.

## 2. Observations & Synoptics [final draft]

### 2.1. Observational Data

According to *Seibert et al.* [2000], if an observation data-set is going to be deployed for testing determination-methods of the mixing-layer depth, it should at least satisfy the following requirements: 1.) sufficiently uniform terrain without too much influence of orography and/or (large) obstacles; 2.) measurements of turbulent fluxes at the surface; 3.) continuous profile information from a remote-sensing instrument, like a RASS-system, as a second (independent) continuous data-source; 4.) radiosonde data of minimal four daily launches. It is clear that these requirements additionally apply to intercomparison studies, like this current one. As a result, the data-set of May 1995 from the Cabauw observational tower (51.99° $N$, 4.93° $E$, 2 $m$ ASL), The Netherlands, is especially suitable for evaluating atmospheric boundary-layer schemes, including surface-flux schemes [*Beljaars and Bosveld*, 1997]. The surrounding land-surface is almost completely flat and the terrain consists mainly of pastures and meadows with interspersed small water channels and thin lines of shallow trees.

During this measuring-period, the development and evolution of the CBL were monitored in detail. In this respect, the sensible heat flux and latent heat flux were measured by the eddy-correlation method. Surface ground-temperature, sea-level pressure, friction velocity, downward shortwave radiation and downward longwave radiation were obtained from measurements with the same frequency. The height of the mixing-layer was observed every 15 $min$ by boundary-layer profile measurements, *i.e.*, an electromagnetic wind-profiler based RASS-system. This remote-sensing device is able to monitor in a direct and continuous way the development and evolution of the mixing-layer in a CBL. Moreover, it appears to be well suited for determining the PBL-depth with Richardson-number methods [*Seibert et al.*, 2000]. In addition, observations of wind, temperature and moisture at eight different heights (from 0.6 $m$ up to 200 $m$ AGL) were carried out at the tower. Except for the remote-sensing measurements, the data-set contains 30-$min$ time-averages for the surface and tower observations. Therefore, all figures presented in this study are plotted at similar time intervals for the corresponding variables.

High-resolution ($\pm$59 $m$) vertical profiles of the same variables were taken every six hours by radiosoundings to complete the measurements. The radiosoundings were launched during the *Tropospheric Energy Budget Experiment* (TEBEX) [*Feijt and Van Lammeren*, 1996; *Raschke and co-authors*, 2001] at KNMI in De Bilt, The Netherlands, which is about 25 $km$ located to the northeast from the site (52.10° $N$, 5.18° $E$). The mixing-layer heights from the radiosonde-data are determined by eye from the resulting vertical profiles of the potential temperature and specific humidity. Hence,

this detailed observational data-set of surface and upper-air measurements will be the reference in this current intercomparison of *MM5*'s boundary-layer parameterizations.

### 2.2. Synoptic Situation

At the beginning of May 1995, a high-pressure system was established over the south of Sweden. As its center was moving southward across the Baltic Sea along the border of Germany and Poland, a small high-pressure zone was simultaneously drifting off from the main system to the coastal area of northern Germany and The Netherlands onto the North Sea where it was decoupled. The presence of the main system provided the optimal conditions to develop a clear (convective and stable) boundary layer over the Cabauw observational tower. During the $2nd$ and $3rd$ of May (hereafter called day 122 and 123), clear CBLs has indeed been observed above the site. The CBLs were characterized by well-mixed thermodynamic variables, larger entrainment rates and high subsequent growth of the mixing-layer. During this period, the main geostrophic winds were easterly to southeasterly with observed, surface wind-speeds of about 1.5–4.5 $m/s$ at 10 $m$ AGL between 6 and 18 UTC (7 and 19 LT) on both days. Apart from the winds resulting from the high pressure-system, a sea-breeze appeared on those days that can influence the development and maintenance of a PBL. Figure 1 shows a *MM5*-output of the wind-field and ground temperatures for the synoptic situation of most of The Netherlands on day 123 at 12 UTC. As the figure shows, the sea-breeze along the north-west coast is reproduced well by the model, which has calculated its penetration to about 20–30 $km$ for both days. Similar sea-breeze penetrations and strengths were indeed observed on both days [*S. Tijm, personal communication,* KNMI, *2001*]. In consequence, it will not effect the simulations of the PBL developments over Cabauw as the site is situated more inland.

**Figure 1.**

## 3. Description of Experiments [final draft]

### 3.1. Model Configuration

For this study, version 3 release 3-2 of PSU/NCAR *MM5* [*Dudhia*, 1993; *Grell et al.*, 1995] is used. A coarse 27-$km$–grid domain covers a part of Northwest-Europe with a domain-size area of 810 $km$ x 810 $km$. Three inner domains — two-way nested — are placed inside the coarse domain, using resolution of 9, 3 and 1 $km$. The second 9-$km$–grid domain covers most of The Netherlands, Northern Belgium and a small part of the sea, resulting in a domain-size area of 270 $km$ x 270 $km$. The third one covers the middle and western part of The Netherlands, in which the smallest one is centered at the Cabauw-tower, resulting in domain-size areas of 90 $km$ x 90 $km$ and 30 $km$ x 30 $km$, respectively.

Figure 2 shows the three domains over the Cabauw-site with the figure's borders representing the coarse domain. The initial and boundary conditions are updated every six hours with meteorological variables calculating from the 0.5° x 0.5° ECMWF-model. For summer conditions of land-surface properties, such as albedo, roughness length and moisture availability, a topography and land-use database of the U.S. Geological Survey (USGS) with 25 categories is used. The resolution of this database for the two outer domains is set to 5 *min* (*i.e.*, about 9 *km*), and for the two inner domains, it is put to 30 *sec* (*i.e.*, about 0.9 *km*). From a total of 26 $\sigma$ model-levels, twenty with an average vertical grid-spacing of 87 *m* are defined inside the ABL. Because the main objective of this study is to analyze solely the performance of the planetary boundary-layer parameterizations, it is decided not to use the model option to nudge surface and radiosonde observations during the simulations, *i.e.*, no four-dimensional data assimilation (FDDA). One or both options will only lead to more complex study-results, which consequently may influence conclusions about the model's physical performance. Additionally, the model should perform reasonable in parts of the world where there is no dense observational network available, like remote areas. Finally, table 1 shows the most relevant physical options within the model configuration that are set for all simulation-runs.

**Figure 2.**

**Table 1.**

### 3.2. Implementation of Experiments

Numerical experiments are set up to investigate, whether *MM5* is able to reproduce the situation described in §2.2. First, two simulations — one with a local PBL-scheme and one with a non-local scheme — are carried out with a minimum of changes in the model's options to determine, if the synoptic situation is to be correctly simulated with most of its *default*-settings (Experiment 1). In addition, two similar simulations are carried out, except that now a *spin-up* time of 24 *h* is included in both runs (Experiment 2). In other words, the model is set up to make a forecast-run from 0 UTC on the 1*st* of May till 0 UTC on the 4*th* of May, 1995.

However, *Oncley and Dudhia* [1995] previously examined the sensitivity to soil-moisture availability for the latent heat flux. From that study, it became clear that the soil-moisture availability has a strong influence on the surface fluxes. Hence, in the third experiment the default moisture availability of 30 % normally provided by the model for the surrounding terrain of Cabauw is modified to a more appropriate value of 60 %. With this higher soil-moisture content, the simulated latent heat flux should agree better with the observations. This experiment (Experiment 3), which is implemented for all four boundary-layer parameterizations, is eventually considered as the *control*-run for all other numerical simulations and, therefore, it will be the starting-point of the discussion in Section 5. For this, the

BRT-scheme can only use its own integrated soil model for ground-temperature predictions. This will make the discussion about the performance of this scheme more difficult, with regard to the other schemes.

The following experiments are solely carried out with MRF. Reasons for this choice are that, first of all, it is the most used PBL-scheme, as it has been most frequently reported in literature (*e.g.*, *Troen and Mahrt* [1986]; *Holtslag and Boville* [1993]; *Warner and Sheu* [2000] and *Hanna and Yang* [2001]) and secondly, it has proven to give reasonably good results in 3D weather-forecast models (*e.g.*, *Chen and Dudhia* [2001a] and *Zhong et al.* [2001]). The next two experiments (Experiment 4 & 5) involve a sensitivity-test about the *roughness length* and a correction in the *land-use* category. The last experiment (Experiment 6) contains two simulations concerning with the impact of different *soil models*. In this case, a closer look is taken to the different behaviour of the so-called *Multi-Layer Soil Temperature Model* (5L-LSM) [*Dudhia*, 1996], which is being used in almost all previous runs, and the *Land-Surface Model* from the *Oregon-State University* (OSU-LSM) [*Chen and Dudhia*, 2001b]. For this experiment, however, data from the NCEP-NCAR's global analysis database (hereafter called NCEP-data) has to be used as OSU-LSM can only be initialized with this database. Therefore, one simulation is carried out with 5L-LSM and the other with OSU-LSM, both using NCEP-data. The purpose of the first run is to help better determine the influence of OSU-LSM on MRF's performance. Table 2 shows all numerical experiments with their names (printed *italic* here) pointing out to the main research-idea.

Finally, the output-data of *MM5* represent 1-$h$ time-and-spacial averages for an area of 1 $km^2$ with a layer thickness of about 87 $m$. Therefore, all figures presented in this study are plotted at similar time intervals for the surface fluxes, or show vertical profiles of an 1-$h$ average state of the PBL. As for the latter, the vertical resolution of the radiosonde data is about two times higher than that of *MM5*. The mixing-layer depth, which is plotted at same time-intervals as the surface fluxes, is estimated for all experiments by calculating the bulk Richardson-number ($R_{iB}$) from the simulated vertical profiles of wind and virtual potential temperature, using a critical Richardson-number of 1.0 as a threshold. **Table 2.**

## 4. Boundary-Layer & Land-Surface Schemes [final draft]

As mentioned before, two local and two non-local PBL-schemes are validated and evaluated using observations. Below, these schemes are briefly described, mainly focusing on their overall characteristics and, more specifically, their treatment of the vertical mixing-process in a CBL over land. In addition, this section will close with a general description of the employed land-surface scheme for calculating the surface variables as it is the link between the PBL-scheme and the soil model in *MM5*.

### 4.1. High-Resolution Blackadar

The *High-Resolution Blackadar* scheme (BLA) incorporated into *MM5* is a revised version of Blackadar's non-local, first-order closure PBL-model, which solves the vertical mixing of horizontal winds ($u$ and $v$), potential temperature ($\theta$), mixing ratio ($q_v$), cloud water ($q_c$) and ice ($q_i$) [*Grell et al.*, 1995]. Two different regimes, which are related to the atmospheric stability, are used for describing this vertical-mixing process: a *stable regime* based on non-local $K$-type closure theory, and a *free-convection regime* derived from the parcel method as practiced in synoptic meteorology [*Blackadar*, 1998]. In other words, ABL-conditions that including stable, mechanically driven turbulence and forced convection are separately treated from the free-convection regime. Although this PBL-scheme is normally classified as a non-local parameterization, it only refers to the free-convection regime. The magnitude of the surface-layer scaling parameter $\zeta = |z_i/L|$ and the sign of the temperature-gradient in the lowest, first model-level determine which of the two regimes will be operational. This will eventually give direction to which equations will be used to calculate the surface-layer stability correction-terms for heat ($\psi_h$) and momentum ($\psi_m$). In all PBL-schemes of *MM5*, prognostic variables ($u, v, \theta$ and $q_v$) are determined at every *half-*$\sigma$ model-level (here: 39 $m$), and diagnostic quantities ($R_{iB}, K, Q_H, Q_E$ and $\tau$) are defined at each *full-*$\sigma$ model-level (here: 79 $m$), where $K, Q_H, Q_E$ and $\tau$ are the eddy diffusivity coefficient, the sensible heat flux, the latent heat flux and the momentum flux, respectively. Phase changes of atmospheric radiation is assumed to occur only at the ground.

The free-convection regime is applied, when $\zeta > 1.5$ and $R_{iB} < 0$. In contrast to local PBL-schemes, vertical mixing in a state of free convection is here being determined by the thermal structure of the ABL and the surface sensible heat flux, instead of local gradients as in $K$-theory. Consequently, in BLA, a simple energy diagram of the profile of potential temperature is being used to diagnose the mixing-layer depth, $z_i$ (*cf. Zhang and Anthes* [1982], Fig. 2). For this, an air-parcel transported upward is assumed to have the surface layer's virtual potential temperature, $\theta_{va}$, which is defined at *half-*$\sigma$ model-level, $z_a$. The rising air-parcel will reach a level where it equals the virtual potential temperature of its surrounding air. This is the height where zero buoyancy occurs, $z_m$, which generally intersects the mixing-layer's capping inversion. The area enclosed by $z_a$ and $z_m$ contains positive (kinetic) energy, $P$. The PBL-depth, however, additionally includes an extra level of overshoot to warrant the effect of entrainment. This results in a greater virtual potential temperature at the top of the mixing-layer than $\theta_{va}$. The area (of overshoot) between $z_m$ and $z_i$ consists of negative (kinetic) energy, $N$. The ratio between $N$ and $P$, which is set to 0.2, is the entrainment rate, $E_m$. Thus, in BLA the values for $P$ and $E_m$ determine the height of the mixing-layer, which is provided as a *MM5*

model-output.

In order to account for the air-parcel's interaction with its entrainment (*cf. Zhang and Anthes* [1982], Fig. 2), during its ascend, at each time-step, a fraction of the air at each level is exchanged between the thermal column and its surrounding air layer. Generally, the fraction decreases with height. Heat, momentum and moisture are exchanged in equal manner at the same time. The fraction at each level is determined by keeping the total net heat transferred from the ascending column to its environment constant with the heat that is transported out of the surface layer, which is defined at a *full-*$\sigma$ model-level, during this time-interval. In this way, the principle of heat energy conservation is preserved. The intensity of the vertical mixing-process, hereby, depends on the sensible heat flux at the top of the surface layer, which is determined by the prognostic variables at the lowest two $\sigma$ model-levels. In conclusion, vertical mixing takes place between the lowest model-layer and the each layer in the mixing-layer aloft.

Above the boundary layer, free atmospheric diffusion is determined by the local $K$-theory approach, in which the eddy diffusivity is a function of the local Richardson-number. It is assumed that no energy flux takes place at the top of the mixing-layer. See *Zhang and Anthes* [1982]; *Grell et al.* [1995]; *Blackadar* [1998] for more details.

### 4.2. Medium-Range Forecast

The *Medium-Range Forecast* scheme (MRF) — available in *MM5* — is the non-local, first-order closure PBL-scheme developed by *Hong and Pan* [1996] as it is implemented in NCEP's Medium-Range Forecast Model. It is based on a previous boundary-layer parameterization developed by *Troen and Mahrt* [1986]. The scheme has certain resemblances with the one of BLA. Correspondingly, it consists of the same two regimes: a stable one and a free-convection regime. Boundary-layer conditions belonging to the stable regime are treated in the exact same manner as in BLA. It differs, therefore, in its treatment of free convection, which is assumed — analogous to BLA— when $\zeta > 1.5$ and $R_{iB} < 0$.

In contrast to BLA, the free-convection regime of MRF takes the contributions from large-scale eddies into account in the local, vertical mixing-process throughout the whole PBL. In this way, the effect of entrainment at the top of the ABL to the mixing process is being introduced. This is accomplished by correcting the profile-gradients in MRF's non-local diffusion scheme with its specific counter-gradient transport terms for temperature ($\gamma_\theta$) or moisture ($\gamma_q$). The counter-gradient terms are defined as:

$$\gamma_\theta = b\frac{\overline{w'\theta'}}{w_s} \quad \text{and} \quad \gamma_q = b\frac{\overline{w'q'}}{w_s} \;, \tag{1}$$

where $b$ is a constant equal to 7.8; and $w_s$ is the convective velocity scale above the surface layer. Furthermore, above the surface layer, the mixing process is realized by bulk-similarity and conditions near the top of the surface layer in conjunction with $K$-type closure theory. In other words, eddies are given the (non-local) bulk characteristics of the ABL, instead of local properties from adjacent layers as in local PBL-schemes. Consequently, the eddy diffusivity for momentum, $K_m$, is obtained from the bulk characteristics of the ABL by a function of $w_s$. The eddy diffusivities for temperature, $K_h$, and moisture, $K_q$, are thereupon being computed from $K_m$ using a Prandtl-number relationship. Hence, the scheme's general turbulent diffusion equation is calculated from the eddy diffusivity coefficient and the corrected gradient by:

$$\frac{\partial C}{\partial t}|_{PBL} = \frac{\partial}{\partial z}\left[K_C\left(\frac{\partial C}{\partial z} - \gamma_c\right)\right] \ , \tag{2}$$

where $C \in (u, v, \theta, q_v)$, and $K_C$ and $\gamma_c$ are the specific eddy diffusivity and counter-gradient term for momentum or temperature, respectively. Like in BLA, the intensity of the vertical mixing depends on the sensible heat flux at the top of the surface layer.

MRF additionally contains a modified equation to determine $z_i$ derived from the bulk Richardson-number equation. It was incorporated into MRF by *Hong and Pan* [1996] to include the effects of rising thermals in the ABL via its surface heat fluxes. The PBL-height is calculated according to $z_i = R_{ic}[\theta_{va}\overline{M}(z_i)]/(g[\theta_v(z_i) - \theta_s])$, where $\overline{M}(z_i)$ and $\theta_v(z_i)$ are, respectively, the wind-speed and virtual potential temperature at the top of the PBL, and $\theta_s = \theta_{va} + \theta_T$ is a near-surface potential temperature, in which $\theta_T$ is a scaled virtual potential temperature excess near the surface. All remaining symbols assume their usual meteorological meaning, where "$a$" refers to the first (half-) $\sigma$ model-level.

As in BLA, above the mixing-layer, local $K$-type theory, in which the eddy diffusivity is a function of the local Richardson-number, is being implemented for solving the vertical turbulent transport in the free atmosphere. See *Troen and Mahrt* [1986]; *Hong and Pan* [1996]; *Braun and Tao* [2000] for more details.

### 4.3. Eta-Mellor-Yamada

The *Eta-Mellor-Yamada* scheme (Eta) implemented in *MM5* is a modified version of the boundary-layer parameterization in NCEP's Eta-model. This scheme is derived from the one employed in the Step-Mountain $\eta$-Coordinate Model of the U.S. National Meteorological Center (NMC). The Eta-scheme in *MM5* is a local PBL-scheme in which turbulent fluxes are closed by $K$-theory regimes to calculate and predict the turbulence kinetic energy (TKE). This scheme is often called the Mellor-Yamada level 2.5-closure scheme. Over water surfaces, it additionally has a sophisticated viscous sub-layer at the

bottom of the surface layer. Eta computes the turbulent, vertical diffusion of $T, \theta_v, u$ and $v$ with an implicit diffusion-scheme.

Compared to MRF, the profile-gradients in Eta's general turbulent diffusion equation (*cf.* Eq. 2) are not corrected by counter-gradient terms. Turbulent fluxes are proportional to the mean gradients and an exchange coefficient for momentum, $K_m$, or heat, $K_h$, that depend on the TKE and a master length-scale. The specific humidity is considered to be a passive quantity ($K_q = K_h$), because phase-changes of atmospheric water affect the turbulence indirectly through variations of the large-scale driving parameters. The TKE is being initialized by the level 2.5-closure scheme from above within the PBL. In this way, Eta can respond quickly to possible large thermal instabilities in the initial conditions and to accelerate the ABL spin-up. In contrast to the original scheme developed by *Janjić* [1990, 1994], *MM5*'s version of the Eta-scheme does not include a separate Mellor-Yamada level 2-closure scheme for the surface layer with a logarithmic dynamical turbulence layer at its bottom. Instead, the Monin-Obukhov similarity theory (*i.e.*, standard stability-functions) involving a counter-gradient fix is used for representing the surface layer in the model. In addition, the scheme is amended for using an effective roughness length.

Unlike the non-local schemes, Eta does not determine $z_i$ as *MM5*-output. Above the ABL, the level-2.5 scheme is additionally being applied to the vertical mixing in the free atmosphere. See *Janjić* [1990, 1994] for more details.

### 4.4. Burk-Thompson

The *Burk-Thompson* scheme (BRT) available in *MM5* is a modified version of the PBL-scheme developed by *Burk and Thompson* [1989]. Parameterization is based on the local, level 2.5-closure scheme of Mellor-Yamada with a separate surface-layer scheme over water surfaces, in conjunction with $K$-type theory. As in Eta, BRT calculates and predicts the TKE. In this scheme, prognostic equations for temperature variance ($\overline{\theta_l'^2}$), moisture variance ($\overline{q_w'^2}$), and temperature-moisture covariance ($\overline{\theta_l' q_w'}$) are included, which are necessary for the evaluation of generalized eddy coefficients. Although both schemes have different parameterizations at the bottom of the ABL over water surfaces, in *MM5* BRT and Eta have certain similarities.

For closing the set of equations, BRT's general turbulent diffusion equation equals the one of Eta. In contrast to what is stated in *Burk and Thompson* [1989], *MM5*'s version of the BRT-scheme does not take the effect of liquid water into account along with the exclusion of the counter-gradient terms in the fluxes for heat and moisture. The eddy diffusivity coefficients $K_m$ and $K_h$ in Eta are differently

calculated than in BRT that relates them to complex algebraic functions that imply the predicted mean and turbulence variables. Furthermore, instead of obtaining $K_q$ via a function of the vertical velocity variance as in the original version of BRT, in *MM5* it is a product of $K_h$ and the Schmidt-number. This is given by $K_q = Sc \times K_h$, where $Sc$ is equal to 1.0075. In addition, BRT and Eta employ virtually the same values for the empirical closure-constants, mainly differing in the number of significant figures (about 2 and 18 for BRT and Eta, respectively).

Like Eta, BRT does not provide a *MM5*-output of $z_i$. Above the mixing-layer, the same scheme additionally accounts for the vertical turbulent transport in the free atmosphere. See *Burk and Thompson* [1989]; *Braun and Tao* [2000] for more details.

### 4.5. Land-Surface Scheme

In order to compare four boundary-layer schemes under equal conditions, the same land-surface scheme is applied to all experiments. Next to the fact that it is the link between the PBL-schemes and the soil models in *MM5*, the land-surface scheme is an essential element in determining the nature and behaviour of the ABL. Therefore, it is useful to summarize the relevant parts of the land-surface parameterization, represented by surface fluxes for momentum ($\tau_s$), heat ($H_s$), and moisture ($E_s$). The overall expressions for the surface fluxes read:

$$\tau_s = \rho_a C_D \overline{M}_a^2 \ , \tag{3}$$

$$H_s = \rho_a c_p C_\theta \overline{M}_a (\theta_g - \theta_a) \ , \tag{4}$$

$$E_s = \rho_a L_v A_m C_q \overline{M}_a [q_{vs}(T_g) - q_{v\,a}] \ , \tag{5}$$

where $C_\theta, C_q, C_D$ are the PBL-scheme's specific drag-coefficients for heat, moisture and momentum, respectively; $A_m$ is moisture availability (a constant provided by the selected Land-Use/Vegetation database in the model); and $q_{vs}(T_g)$ is the saturation vapor mixing-ratio at surface as a function of the surface temperature. For the latter, the general approximation by a variation of the Teten's formula reads [*Stull*, 1988]:

$$q_{vs}(T_g) = \frac{0.6112\epsilon}{p} \exp\left[\frac{17.67(T_g - 273.15)}{T_g - 29.66}\right] \ , \tag{6}$$

where $\epsilon = 0.622\ g/g$ is the ratio of gas constants for air and water vapor, and $p$ is the air pressure in $kPa$. All remaining symbols assume their usual meteorological meaning. The differences between the PBL-scheme are, hereby, being reduced to the prescription of the three drag coefficients: $C_D$, $C_\theta$ and $C_q$.

In the land-surface scheme, ground-temperature predictions — regarding $\theta_g$, $T_g$ and $q_{vs}(T_g)$ — are performed by the selected soil model in *MM5*. However, as mentioned before, BRT can merely function

with its own integrated force-restore soil model. Meaning that BRT takes the ground-temperature predictions for its part, while the other PBL-schemes interact with the separate soil models available in *MM5* like, for instance, 5L-LSM and OSU-LSM.

## 5. Results & Discussions [final draft]

As mentioned before, the observed CBLs of day 122 and 123 at the Cabauw-site are modelled by *MM5* along with a sensitivity-test for each of the model's PBL-schemes discussed in the previous section. From a synoptic point of view, the forcing that drives the evolution and development of the ABL are the heat and moisture flux at the surface, and the entrainment flux at the boundary-layer top. For the surface variables, the partitioning of the incoming radiation into sensible and latent heat flux is a determining factor. In this context, examining the near-surface variables will give insight into the interactions between the land-surface schemes and PBL-schemes in *MM5*. The entrainment of warmer air from the free troposphere into the ABL specifically contributes to its heating and its drying. The growth of the PBL mainly depends on these bottom and top boundary-layer fluxes in a convective case. However, in somewhat less ideal circumstances, non-local effects, like advection of heat, moisture and momentum, and subsidence can additionally have considerable influence on the growth of the mixing-layer depth.

### 5.1. Surface Fluxes

Figure 3 and 4 show the observed and simulated diurnal cycles of the sensible heat flux, $H$, and the latent heat flux, $E$, respectively. All four PBL-schemes in *MM5* overestimate the sensible heat flux during day-time, particularly those predicted by the non-local schemes. Similar results were found by *Chen and Dudhia* [2001a] for MRF. Note that the observations are relatively low for $H$, concerning the time of season. Evaporation is probably a cause for this as the surrounding terrain at the Cabauw is rather humid. However, uncertainties in the observations may probably be an additional cause as they have been determined by the eddy-correlation method [*F.C. Bosvelt, personal communication,* KNMI, *2001*]. This method is known to be sensitive for measurement errors [*Stull*, 1988]. Compared to the local parameterizations, the non-local ones produce about twice the maximum value occurring between 11 and 12 UTC (*i.e.*, 12 and 13 LT), which is about 185 $W/m^2$ (day 122) and 165 $W/m^2$ (day 123). The local schemes calculate maximum values between 70 and 130 $W/m^2$ on both days, with BRT performing rather well at day 123. However, at day 122 during the early morning, the non-local schemes calculate the increase of $H$ more according to the observations, while for the local group positive values of $H$

start approximately an hour earlier. This does not account for day 123, where the early-morning evolution of $H$ calculated by all schemes nearly coincide with the observations. After 12 UTC on both days, the non-local group calculate the decline of $H$ about an hour later. Regarding the local schemes, Eta predicts a slower decline than BRT, which follows closely the non-local schemes. The only clear performance differences between the non-local PBL-schemes occur after mid-day on day 122. The differences between the local schemes are more obvious, where BRT performs better than Eta.

In case of the predicted $E$, all four schemes also overestimate the flux during day-time. However, uncertainties in the observations can probably exist as typical latent heat fluxes for Cabauw at this time of year would be somewhat larger. On both days around mid-day, the non-local schemes perform better with maximum values of about 300 $W/m^2$ (day 122) and 335 $W/m^2$ (day 123), than the local ones that have maximum values between 360 $W/m^2$ and 410 $W/m^2$ on both days. Compared to $H$, the results show an opposite picture, although the differences between the two groups are less prominent. Especially for day 123, where the differences between the non-local schemes are negligible, while those between the local get larger. Though, MRF predicts $E$ more close to the observations compared to all other schemes, where Eta produces higher values than BRT, which seems to show an improvement on day 123. After mid-day, all schemes show an inertia effect in the decline of $E$.

In order to explain these overestimations of both heat fluxes, it is necessary to analyse first the downward short-wave radiation ($K\downarrow$) and downward long-wave radiation ($I\downarrow$). In this context, it is important to bear in mind, however, that in *MM5* the surface-energy balance is preserved in all cases, while this does not usually account for the surface observations. The diurnal cycles of the modelled $K\downarrow$ is reasonably well predicted by all four schemes during both days with negligible performance differences between the schemes (not shown here). Around mid-day, however, all schemes show a slight overestimation with respect to the observations of about 10 $W/m^2$ on day 122 and about 40 $W/m^2$ on the next day. With regard to $I\downarrow$, all schemes simulate it fairly well (not shown here). *Chen and Dudhia* [2001a] have reported similar results for MRF and state that overestimations of $K\downarrow$ are fairly common in mesoscale models under meteorological conditions like the days under study. They stated that the overestimation is probably due to the absence of aerosol treatment in *MM5*'s current radiation scheme. Therefore, the analysis is turned to other, possible reasons causing the discrepancies. As stated earlier, the sensible heat flux and the latent heat flux at the surface are determined by equation 4 and 5, respectively. A close examination shows that, if during day-time, the atmospheric stability stays unchanged (*i.e.*, the free-convective regime is operational), like on the days under study, the following prognostic variables play a role in the determination of the fluxes: the friction velocity ($u_*$),

which is related to the wind-speed ($\overline{M}_a$); the temperature difference ($\theta_g - \theta_a$) for $H$ and the moisture difference $[q_{vs}(T_g) - q_{va}]$ for $E$.

Figure 5 and 6 show the observed and simulated time evolution of the friction velocity, $u_*$, and the wind-speed at 0.6 $m$ AGL, $\overline{M}_{0.6}$, respectively. For $u_*$, it shows that all four schemes largely overestimate this velocity scale during day-time. The non-local group produces somewhat higher maximum values roughly of 0.48 $m/s$ (day 122) and 0.43 $m/s$ (day 123) around 12 UTC, where BLA seems to have tendencies to produce slightly higher values than MRF. The local schemes perform slightly better with maximum values of about 0.41 $m/s$ around mid-day on day 122, while the next day they are significantly closer to the observations (about 0.33 $m/s$). Here, BRT seems to do better than Eta. Note that the local schemes — especially BRT — seem to respond better to the observed $u_*$ than the non-local group. A possible explanation for this is that these local parameterizations calculate the turbulent fluxes as a function of the TKE.

The wind-speed calculations ($\overline{M}$) in the surface layer performed by the schemes disagree largely with the observations, especially the non-local schemes. Close to the earth's surface (Fig. 6), all schemes show tendencies to overestimate $\overline{M}_a$ . It should be note that model-results are compared here to observations at 10 $m$. Similar results for both non-local schemes were reported earlier by *Shafran et al.* [2000]; *Warner and Sheu* [2000]; *Hanna and Yang* [2001] and *Zhong et al.* [2001], who found (occasionally using FDDA) that BLA and/or MRF produced surface wind-speeds having an average mean bias of about 0.5 $m/s$ with a root-mean-square-error (rmse) of about 2–3 $m/s$ or 5–6 $m/s$. In the first 200 $m$ of the PBL, however, all schemes improve their performances. As expected from the calculated $u_*$, the local group respond better to the observed wind-speed in the first 200 $m$. In all cases, a somewhat better agreement is found between the local PBL-schemes and the Cabauw-tower observations than the non-local ones.

Figure 7 and 8 show the observed and simulated diurnal cycles of the ground temperature, $T_g$, and the potential temperature at 0.6 $m$ AGL, $\theta_{0.6}$, respectively. For $T_g$, on both days, the non-local PBL-schemes overestimate $T_g$ by about 1.5°–2° around mid-day. Caution must be taken here, because measurements of $T_g$ contain uncertainties [*F.C. Bosvelt, personal communication,* KNMI, *2001*]. However, the results seem common according what has been reported earlier by *Warner and Sheu* [2000] and *Zhong et al.* [2001], who found for BLA and/or MRF predicted surface temperatures having a mean bias of −1.8°–0.2° with a rmse of about 2.5°. The local ones calculate it slightly closer to the observations during this time, of which BRT shows tendencies of underpredicting $T_g$ on day 123. In addition, all schemes overestimate $T_g$ in the morning, where the local parameterizations reach their

maximum about one hour earlier than the observations or the non-local schemes. On both days, differences between the two non-local schemes are somewhat negligible, where MRF has tendencies to produce higher values than BLA. In case of the local parameterizations, Eta shows significantly higher values (about 1.25° on both days) than BRT (about ±0.5° on both days) during mid-day, particularly for day 123. As all PBL-schemes start with the same ground temperature at 0 UTC, this suggests that $T_g$ is not correctly initialized by ECMWF-data. For predictions of potential temperature ($\theta_{0.6}$) in the surface layer (Fig. 8), differences between the schemes mentioned before for $T_g$ can additionally be found here, except now all PBL-schemes underpredict $\theta_{0.6}$ during day-time, especially the local ones. Compared to the observations, the modelled temperatures are lower during the day and with a temporal shift in the maximum of approximately two hours later.

Figure 9 shows the observed and simulated time evolution of the near-surface specific humidity at 0.6 $m$ AGL, $q_{v0.6}$. All four schemes calculate the evolution of $q_{v0.6}$ with considerable error. None of the PBL-schemes — especially the non-local ones — are able to capture the increased and decreased surface humidity during day-time and night-time, respectively. On both days, though, the local schemes are somewhat better in capturing the surface-humidity increase right after sun-rise and in the late afternoon than the non-local ones. These humidity-increases are probably due to, respectively, the emergence of the observed mist (day 122) and evaporation of morning dew (day 123), and the evapotranspiration in the late afternoon (both days). Here, the non-local parameterizations seem to have a tendency of slightly underestimating the specific humidity, particularly on day 123, while the local ones seem to do otherwise.

Thus, returning to equations 4 and 5, it may be clear that $u_*$ (and $\overline{M}_a$) and $q_v$ predicted by *MM5* with the four schemes have considerable influences on the results of the predicted $H$ and $E$ of day 122 and 123. This especially concerns $u_*$ that is implicitly found in both equations in the form of $\overline{M}_a$, and the drag coefficients for heat ($C_\theta$) and moisture ($C_q$). In case of $H$, the temperature difference ($\theta_g - \theta_a$) in equation 4 also plays a relevant part as it contains a considerable bias, resulting form the overestimations of $T_g$ and the underestimations of $\theta_a$ during day-time. Although it is difficult to estimate the feedback between the variables, a sensitivity analysis is carried out on the role of $u_*$ to the estimation of fluxes. By lowering $z_0$, the friction velocity decreases significantly during day-time, as expected. Simultaneously, a small increase of $T_g$ is seen around mid-day, which would have resulted in a higher $H$. Instead, the lower values of $u_*$ lead to a significant, but small reduction of $H$, while no change occurs in the diurnal cycles of $E$. Furthermore, $C_\theta$ must have a considerable impact on the performance of the PBL-schemes as the drag coefficient dependents on, among others, $u_*$ and $z_0$. The

remaining variables in equation 4 can be considered constant. Therefore, the overestimations of $H$ must be effected mainly by the large disagreement of the predicted $u_*$ through $\overline{M}_a$ and $C_\theta$, provided that a corrected, average value of $z_0$ is employed. In this study, a value of 0.15 $m$ is used (Tbl. 2), which is a good representation of the average roughness length found at Cabauw (0.05–0.3 $m$).

With regard to $E$, both variables in the moisture difference $[q_{vs}(T_g) - q_{va}]$ of equation 5 have somewhat the same effect on the flux. It may be clear from the results of the overestimated ground-temperature that $q_{vs}(T_g)$ contains a certain positive bias during day-time as it is a function of $T_g$ (Eq. 6). Simple calculations with equation 6 show that this bias can be considerably large, and, therefore, it may not be neglected. In addition, the errors occurring with $q_{va}$ can have equal (positive or negative) bias compared to $q_{vs}(T_g)$ that result in significant errors of the term $[q_{vs}(T_g) - q_{va}]$. For instance, on day 123, the non-local schemes underpredict $q_{v0.6}$ largely around mid-day (Fig. 9), while higher up in the surface layer estimations get better. This implies a smaller, but still large underprediction of $q_{va}$. At the same time, the error of $q_{vs}(T_g)$ stays somewhat constant as the overestimations of $T_g$ are nearly unchanged compared to the previous day (Fig. 7). Consequently, the humidity-term in equation 5 must be larger than on day 122 at the same time. Additionally, compared to day 122, $u_*$ shows slightly lower values for the non-local schemes on day 123 (Fig. 5), which would have lead to lower $E$ according to equation 5. However, the strength of underpredicted $q_{va}$ results in a larger $E$ for the non-local schemes on day 123.

As was previously found by *Oncley and Dudhia* [1995] for BLA in *MM5*, the moisture availability ($A_m$) in equation 5 has large effects on the performance of the PBL-schemes. The Default-run with MRF and Eta (Tbl. 2) confirms this, especially regarding both heat fluxes and ground temperature. The experiment shows that by lowering $A_m$ to a (unrealistic) default value of 30 %, both schemes show about 40–60 % higher values for $H$ around mid-day, while $E$reduces by about 25–35 % around 12 UTC. For $T_g$, the two schemes overpredict $T_g$ more by about 1.5–2.5° around mid-day. With regard to the performances of both PBL-schemes, only Eta shows an improvement for $E$ here. Like for $H$, the effect of the drag coefficient, $C_q$, cannot be neglected here as $C_q$ dependents on, among others, $u_*$ and $z_0$. The remaining variables in equation 5 are considered constant. Therefore, the appearing bias of $u_*$ through $\overline{M}_a$ and $C_q$, and of term $[q_{vs}(T_g) - q_{va}]$ have considerable effect on the results of $E$ (and $H$), provided that a realistic value of $A_m$ for the Cabauw-conditions (60 %) is used.

In the previous analysis, it is shown that surface variables play a key-role in the flux determination. It is, therefore, convenient to determine the sensitivity of the PBL-schemes to the land-surface scheme. As mentioned before, in order to study this, the Soil-Model experiment with MRF (Tbl. 2) is conducted

in conjunction with OSU-LSM, which is a more sophisticated soil model. *Chen and Dudhia* [2001a] reported a similar study using the FIFE-1987 data for validation against Blackadar's force-restore soil model. They found good performances, especially concerning both heat fluxes, ground temperature and near-surface humidity. However, regarding the surface fluxes, in this study results mainly show minor improvements.

The Soil-Model experiment shows that the overall performance of MRF presented in the previous figures stays unchanged in case of using OSU-LSM, instead of 5L-LSM. OSU-LSM shows only small improvements for both heat fluxes, with maximum reductions of about 13 % and 11 % at mid-day for $H$ and $E$, respectively. All other surface variables show increased overpredictions, particularly $u_*$ and $T_g$ with maximum increases of about 18 % and 3° at mid-days, respectively. For the near-surface variables, no improvements are seen for $\theta_{0.6}$. The time evolution of $\overline{M}_{0.6}$ disagrees more, while $q_{v\,0.6}$ shows a slight improvement in capturing its diurnal characteristic evolution. However, while the average, daily surface humidity seems to increase in time, OSU-LSM calculates an opposite trend.

**Figure 3.**

**Figure 4.**

**Figure 5.**

**Figure 6.**

**Figure 7.**

**Figure 8.**

**Figure 9.**

### 5.2. Vertical Profiles

Figure 10 shows the comparison of the calculated and observed vertical profiles of potential temperature at 12 UTC for day 122. At this time of day (*i.e.*, 13 LT) on day 122, the non-local PBL-schemes reproduce the vertical structure of the CBL reasonably well and agree considerably better with the observations than the local ones. With respect to the time evolution of the vertical profiles on day 122, previous observed profiles (6 UTC; not shown here) show negligible differences between the schemes, where all schemes capture well the observed, vertical structure of the stable PBL, characterized by a surface-inversion. In other words, the large-scale initial and boundary conditions of the lower atmosphere at the start of the simulation (0 UTC) is well reproduced. Above the inversion, all four schemes show a cold temperature bias (approximately 2°) which becomes smaller during the rest of the morning.

By 12 UTC, all four schemes still show about 0.7° and 1.5° for the non-local and local schemes, respectively, colder CBLs than the observations, where the local schemes have additionally lower capping inversions. *Zhong et al.* [2001] found similar results for MRF and BLA compared to observations of the VTMX-2000 field campaign. For the current study, this is a contradictory result since the sensible heat fluxes are being overestimated by the schemes, which should result in a warmer CBL compared to the observations. This may imply that the interaction between the surface and the PBL is not correctly parameterized for effectively transferring the overestimated $H$ to the air above. Although, a higher

vertical resolution of the model could be the solution to get the vertical profile more in line with the predicted $H$. *Hanna and Yang* [2001] has also suggested higher vertical resolutions to achieve a performance enhancement in predicting the vertical structure. The local schemes produce the coldest ABLs with the lowest entrainment zones as well as the lowest values for the sensible surface flux (Fig. 3). A possible explanation is that these schemes are unable to produce sufficient turbulent motions for creating a well-developed CBL. At this time of day, differences between the (non-) local schemes are mainly significant at the top of the CBL. Note that the vertical resolution of *MM5* is too course for the schemes to resolve the super-adiabatic temperature profile at the bottom of the observed CBL. During its warming up in the rest of the afternoon, the observed CBL deepens faster than the modelled ones. At the same time, the cold bias of both local schemes becomes larger again and differences between the (non-) local schemes get more apparent.

At 18 UTC, the observed ABL has a higher mixing-layer depth than at mid-day (not shown here). The cold bias of the local schemes is increased to about 2.5°, while the one of the non-local parameterizations is more or less unchanged. With regard to the calculated level of the capping inversions, the positions have mainly maintained the same as at 12 UTC, where the local schemes underestimate them more than the non-local ones. At this time, all schemes capture fairly well the transition of the nocturnal boundary-layer represented by the surface inversion at the bottom of the ABL.

The next day (day 123), all four schemes in *MM5* reproduce the day-time development of the vertical distributions of $\theta$ in the CBL in a similar kind of way as the preceding day, except that differences seen at day 122 are larger here. At 12 UTC on day 123, all schemes show larger cold biases with larger underestimations of the inversions than the day before, while the observations shows higher temperatures with a lower, but more distinct capping inversion at this time than day 122.

In general, despite of the underestimations of the level of capping inversions and the cold temperature bias by the non-local schemes, they perform better throughout the whole simulation-run of 48 $h$ than the local schemes. During this time, the difference between the simulated and observed temperatures is less than 2°. According to *Chen and Dudhia* [2001a], this is an indication for a good performance of the non-local PBL-schemes. Next to this, they capture better the structure of the vertical profiles than the local counterparts. The vertical profiles show that the exchange coefficient calculated from TKE (local schemes) are relatively smaller under convective conditions and — in consequence — tend to produce less vertical mixing. Additionally, the non-local schemes treat the entrainment of dry air from the free atmosphere more effectively by utilizing an entrainment routine in their schemes,

which is realized for BLA by the entrainment rate, $E_m$ (see §4.1) and for MRF by the countergradients (Eq. 1) in its turbulence diffusion equation (Eq. 2).

Figure 11 shows the comparison of the simulated and observed vertical profiles of specific humidity for the same time and day. As can be expected from the overestimations of the latent heat flux and the results of the vertical temperature profiles (Fig. 4 & 10), all four schemes in *MM5* calculate a more humid CBL than the observations, especially the local PBL-schemes. *Zhong et al.* [2001] reported similar results for MRF and BLA. The time evolution shows that, at 6 UTC (not shown here), all schemes reproduce the observed, vertical distribution of humidity reasonably well, except at the bottom of the ABL where the model-results show an inversion. The inversion is not found in the observations, which show a larger decrease in the first 200 $m$ of the ABL. Differences between the schemes are negligible here.

An additional phenomenon can create a discrepancy between 6 and 12 UTC: While after about 9 UTC (Fig. 9), the observed, specific humidity decreases rapidly with lower inversions, the schemes respond too slow to this development and eventually show an larger disagreement of $q_v$ at 12 UTC than in the morning (6 UTC). The observed decrease could be explained by the fact that mist was observed in the early hours after sun-rise on day 122, disappearing between 6 and 9 UTC. The behaviour of both scheme groups can be explained, when taking the evolution of the overestimations of $E$ (Fig. 4) into account. In other words, as the morning develops, overestimations of $q_v$ calculated by the schemes become larger, where the local schemes produce somewhat the largest, like their latent heat fluxes.

At 12 UTC, the non-local schemes capture the vertical structure of humidity fairly well with an overestimation in the bulk of the ABL compared to the observations of about 2 $g/kg$, whereas the local PBL-schemes show a difference of about 3 $g/kg$. However, the non-local schemes slightly overestimate the inversion at the top of the CBL, where the local ones underestimate it. Differences here between the (non-) local schemes are somewhat negligible, except that BLA is not capable of predicting the small slope of the surface-layer. During the afternoon, the schemes calculate a decrease of $q_v$ in the bulk of the ABL, while performance differences start showing between the schemes. At the same time, the observed $q_v$ deepens further into a well-developed CBL.

At 18 UTC, the observations shows a deeper and slightly more humid CBL than at mid-day (not shown here). Although all schemes predict considerable lower specific humidities than at mid-day, the model results still show overestimations, while the positions of the inversions at the mixing-layer top are unchanged for all schemes. BLA more or less coincides here with the observations, except for the too low inversion. MRF, however, still overestimates $q_v$ by about 1 $g/kg$, but predicts its inversion at the

same height as BLA. This may imply that MRF calculates the entrainment rate too low to get drier air from above. This issue has additionally been reported by *Chen and Dudhia* [2001a]. BRT predicts about 1.5 $g/kg$ more humidity in the CBL compared to the observations, while Eta (except for its inversion) predicts $q_v$ close to MRF.

The following day (day 123), the general performance differences between the two scheme groups in *MM5* are unchanged, although the differences are more apparent. In other words, the non-local schemes — especially MRF — additionally capture the day-time development of the vertical distributions of specific humidity better than the local ones. In addition, the non-local schemes predict $q_v$ now somewhat closer to the observations than the local parameterizations. However, the inversion at the top of the ABL are still mostly underestimated by all schemes, particularly concerning the local ones. At 12 UTC, all parameterizations overpredict $q_v$ considerably less than on the previous day, although the results show for all schemes a larger underprediction of the inversion at the top. At the same time, compared to day 122, the observations shows a less well-mixed CBL with slightly higher $q_v$ and a shaper and higher inversion at the top.

With regard to the impact of OSU-LSM on the performance of MRF, the Soil-Model experiment (Tbl. 2) shows that in *MM5* for both days, OSU-LSM lead to no considerable improvements in the prediction-biases of the vertical distributions of potential temperature and specific humidity compared to the observations. For $\theta$, the vertical profiles calculated with OSU-LSM show throughout the 48 $h$ of simulation the vertical structures are reasonably well reproduced with (occasionally minor) underpredicted capping inversions. For $q_v$, OSU-LSM leads to minor improvements in the overpredictions on day 122, while on the next day it results in the opposite, which is characterized by somewhat larger biases of underpredictions. The cause is probably the downward trend seen in the daily average, near-surface humidity, $\overline{q}_{v0.6}$ (see §5.1). In all cases, however, OSU-LSM leads to better mixed PBLs and a better predictions of the vertical structure, except for the underpredictions of the inversion level and the larger disagreement in the structure at morning-periods (6 UTC).

**Figure 10.**

**Figure 11.**

### 5.3. Mixing-Layer Depths

Figure 12 shows the observed and simulated time evolution of the mixing-layer height for day 122 and 123. All schemes in *MM5* underpredict the maximum PBL-depth during day-time on both days. *Zhong et al.* [2001] found similar results for MRF and BLA. In this case, the Soil-Model experiment with OSU-LSM (Tbl. 2) has shown no significant improvements for MRF on both days. However, the observed, rapid growth of the CBL between 9 UTC and 12 UTC on both days is modelled reasonably well by all

four schemes. Most notable is that all schemes show considerably better performances on day 122 resulting in clear diurnal cycles than on the next day, which is probably related to the somewhat different synoptic situation on day 123.

With regard to day 122, the non-local schemes show smaller underestimations at maximum depth (about 250 $m$) than the local ones (about 450 $m$), where the times of maximum depth are predicted about two hours earlier than the observations. There are no major performance differences between the (non-) local schemes during day-time. The performance of the non-local schemes is a consequence of the better calculated vertical profiles of potential temperature by these schemes, while for the local ones the predicted weak turbulent motions results to the underestimations by those schemes.

On day 123, the simulated boundary-layers are unexpectedly more shallow with underestimations of about 450 $m$ and 600 $m$ for the non-local and local schemes, respectively. However, *MM5* shows a similar trend in the daily maximum PBL-depth compared to the observations, where the observed depth of day 123 is about 200 $m$ lower than on the previous day. In addition, the non-local schemes reproduce well the decay of the observed mixing-layer height after 14 UTC (*i.e.*, 38 UTC in Fig. 12). Compared to day 122, the underestimation has increased here for each scheme by about 200 $m$, whereas the difference of predicted maximum depths between the two scheme groups (about 225 $m$) has stayed somewhat constant.

This might suggest that non-local synoptic effects of day 123 are not well reproduced by *MM5*, and therefore, this can be a cause for these lower performances of all schemes on this day. The influence of advection and/or subsidence can lead to discrepancies in the mixing-layer height predictions due to the incorrect calculations of the wind speed and direction, temperature and moisture. Because of the complexity of feedbacks on the development of the PBL, a brief analysis follows on these related variables for both days.

For the wind speed in the bulk of the PBL, $\overline{M}$, the radiosonde observations show that the observed wind-speeds are larger during the afternoon on day 123 than at the same time on day 122. However, in *MM5* an opposite pattern is predicted: all schemes calculate lower $\overline{M}$ on day 123 than for day 122. For day 123, the modelled wind profiles show large underestimations for $\overline{M}$ and disagree largely with the observed vertical structures. In this respect, *Hanna and Yang* [2001] states that the uncertainties in wind speeds are primarily due to random turbulent processes that cannot be simulated by mesoscale models, like *MM5*, and to subgrid variations in terrain and land use. It is, therefore, unlikely according to them that the errors can be reduced much further.

With regard to the subsidence velocity, $w_L(z_i)$, from the radiosonde observations, it is estimated

that $w_L(z_i)$ is larger on day 123 (about $-0.018\ m/s$) than on day 122, while it increases during day 122 and develops to a maximum at the morning of day 123. In *MM5*, the values between 11 and 16 UTC are also larger on day 123 than on the preceding day, where it ranges from $-0.016$ to $-0.142\ m/s$ for day 123. In addition, on day 123 after 11 UTC, all schemes calculate subsidence for the whole PBL. However, instead of at the morning of day 123 as found in the observations, all schemes predict the minimum value ($-0.041$ to $-0.169\ m/s$) after 16 UTC for this day. The magnitude indicates that *MM5* overestimates $w_L(z_i)$ for day 123 largely. The role of entrainment has not been quantitatively examined in this study. As a first indication, the radiosonde observations show that throughout the whole day, stronger capping inversions exist on day 123 than on day 122. However, all schemes in *MM5* show an opposite development: predicted capping inversions are mostly stronger on day 122 than on day 123.

These discrepances of horizontal and vertical motion must be related to the evolution of the high-pressure system at day 123 (see §2.2). Weather charts show that the observed surface wind-directions on day 122 are reasonably well calculated by *MM5*. Same charts for day 123, however, show that from 15 UTC on, the observed surface winds turn to the north slowly stretching out over the whole country, because of the small high-pressure zone that drifts off onto the North Sea (see §2.2). In spite of *MM5*'s correct prediction of this development, it has underestimated the strength of this small system resulting in wind directions from the east to northeast till the end of the afternoon. This must have effects on the evolution of the PBL at Cabauw as to the north of it the IJsselmeer (an artificial lake that is directly bounded to the north by the North Sea) may bring cooler and moister air (see for situation Fig. 1). However, the latter has not been further examined.

This could mean that temperature advection, $\overline{U_j}(\partial\overline{\theta}/\partial x_j)$, plays a role in the development and maintenance of the mixing-layer height for day 123. In order to determine the importance of the advection term with respect to the heat flux divergence, $-\partial(\overline{w'\theta'})/\partial z$, and the temperature-rate change of the mixing-layer, $\partial\overline{\theta}/\partial t$, calculations are carried out with simulation results from the Control-run (Tbl. 2) with MRF. It was found that on day 122 the temperature advection has a similar order of magnitude than the flux divergence, which is about 0.6 $K/h$. On day 123, temperature advection is about 60 % lower, while the flux divergence is more or less unchanged. Hence, temperature advection cannot be neglected for both days.

**Figure 12.**

## 6. Conclusion & Recommendations [final draft]

Within the context of air-quality modelling, the overall objective of this current study has been to investigate for a clear convective case the performance of four atmospheric boundary-layer schemes

in *MM5* by comparison to detailed surface and upper-air observations, with regard to the ability of reproducing realistic mixing-layer depths during day-time. The investigated ABL-schemes are widely used and can be grouped into local and non-local descriptions of the PBL.

With regard to the surface variables, three main outcomes can be extracted from the results for the days under study (*i.e.*, *2nd* and *3rd* of May, 1995) at the Cabauw-site. As expected, each PBL-scheme belonging to a group (*i.e.*, local or non-local) show similar results. The local schemes give better results compared to the observations for most surface variables during day-time than the non-local group, while an opposite behaviour is found for the latent heat flux. However, all PBL-schemes in *MM5* overestimate both heat fluxes compared to the observations. These overestimations cannot only be justified by the fact that the surface fluxes are measured by the eddy-correlation method as the maximum calculated values by all schemes around mid-day are much large than the expected fluxes for the investigated time of year at Cabauw. Therefore, after prescribing the realistic values of the roughness length and the moisture availability, it has been shown here that the overestimations must additionally be caused mainly by the large overestimations of the friction velocity, the near-surface wind-speed, the temperature difference and moisture difference between the ground and the surface layer for the sensible heat flux and the latent heat flux. The use of a more complex soil model (*i.e.*, OSU-LSM) does not show considerable improvements for MRF, which means that the overall performance of stays unchanged using OSU-LSM, instead of 5L-LSM. OSU-LSM shows only small improvements for both heat fluxes.

For the vertical profiles, on both days all four PBL-schemes calculate colder and more humid CBLs with underestimations of the capping inversions compared to the observations. For the potential temperature, underestimations are larger on the *3rd* of May than on the *2nd* of May. For the specific humidity, all schemes calculate it closer to the observations on the *3rd* of May than on the *2nd* of May, but with larger underestimations of the inversion at the top of the PBL. Regarding the potential temperature, the results are relatively contradictory since the calculated surface heat fluxes are higher, than the observed values. However, it can be an indication of the inadequate modelling of the entrainment flux at the top of the CBL and/or the improper parameterization of the interaction between the surface scheme and each PBL-scheme. In this comparison study, it is additionally found that the local PBL-schemes — Eta and BRT — which depend on the TKE-variable, produce the coldest and wettest boundary-layers, since the modelled turbulent motions are not strong enough to model a well-developed CBL. The better performance of the non-local schemes here are mainly a consequence of the fact that these PBL-schemes describe the vertical mixing between non-adjacent layers in the PBL

and that the entrainment process at the top of the PBL is taken into account by these schemes. This results in better mixing throughout the whole ABL by better representation of large-eddies in convective layers. With regard to the impact of OSU-LSM on the performance of MRF in *MM5*, OSU-LSM leads to no considerable improvements in the vertical distributions of potential temperature and specific humidity compared to the observations of both days. However, it leads to better mixed CBLs and a better predictions of the vertical structure, except for the underpredictions of the inversion level and the larger disagreement in the structure at morning-periods.

For the day-time boundary-layer heights, all schemes in *MM5* underestimate the CBL-depth on both days considerably. The results of the non-local schemes, MRF and BLA, agree better with the observations. Although *MM5* shows a similar downward trend in the daily maximum PBL-depth compared to the observations, all schemes calculate the evolution of the CBL less ideal with larger underestimations on the $3rd$ of May. This is probably associated with the different synoptic situation on this day. As the performance differences between the two scheme groups stay unchanged compared to the previous day, it is suggested that advection, subsidence and/or entrainment are not well reproduced by *MM5* for this particular day. From a brief analysis, it is found that there are discrepancies in the modelled horizontal and vertical wind-speeds compared to the observations which must be related to the incorrect simulation of the synoptic developments of the surface winds by *MM5* on the $3rd$ of May. Calculations indicate that temperature advection cannot be ignored.

In conclusion, this study has shown that the CBL modelled by *MM5* strongly depends on the selected boundary-layer parameterization, where the non-local schemes perform generally better for the vertical profiles and the predicted day-time mixing-layer depths than the local schemes. Therefore, for predictions of mixing-layer heights in CBLs with *MM5*, it is recommended to use non-local schemes for air-quality modelling. Moreover, future work with *MM5* may be addressed to correcting the overestimations of the surface fluxes (*Pagowski and Moore* [2001]); studying the role of the entrainment flux and its description in mesoscale models, and studying interaction and feedback between land-surface and boundary-layer schemes.

## References


Beljaars, A. C. M., and F. C. Bosveld, Cabauw data for the validation of land surface parameterizations schemes, *J. Climate*, *10*, 1172–1193, 1997.

Berman, S., and J. Y. K. S. T. Rao, Spatial and temporal variation in the mixing depth over the northeastern united states during the summer of 1995, *J. Appl. Meteorol.*, *38*, 1661–1673, 1999.

Blackadar, A. K., Modelling the nocturnal boundary layer, in *Third Symp. on Atmospheric Turbulence, Diffusion and Air Quality, Raleigh, NC, Amer. Meteor. Soc.*, pp. 46–49. 1976.

Blackadar, A. K., *Turbulence and Diffusion in te Atmosphere, Lectures in Environmental Sciences.* Springer-Verlag, Berlin, Germany, 1998.

Braun, S. A., and W. K. Tao, Sensitivity of High-Resolution Simulations of Hurricane Bob (1991) to Planetary Boundary Layer Parameterizations, *Mon. Wea. Rev.*, *128*, 3941–3961, 2000.

Burk, S. D., and W. T. Thompson, A vertically nested regional numerical weather prediction model with second-order closure physics, *Mon. Wea. Rev.*, *117*, 2305–2324, 1989.

Chen, F., and J. Dudhia, Coupling an Advanced Land Surface-Hydrology Model with the Penn State–NCAR MM5 Modeling System. Part II: Preliminary Model Validation, *Mon. Wea. Rev.*, *129*, 587–604, 2001a.

Chen, F., and J. Dudhia, Coupling an Advanced Land Surface-Hydrology Model with the Penn State–NCAR MM5 Modeling System. Part I: Model Implementation and Sensitivity, *Mon. Wea. Rev.*, *129*, 569–585, 2001b.

Dudhia, J., A nonhydrostatic version of the Penn-State-NCAR mesoscale model: validation tests and simulation of an Atlantic cyclone and cold front, *Mon. Wea. Rev.*, *121*, 1493–1513, 1993.

Dudhia, J., A Multi-Layer Soil Temperature Model For MM5, in *The Sixth PSU/NCAR Mesoscale Model Users' Workshop*, Boulder (CO), USA. pre-print, 1996.

Feijt, A., and A. Van Lammeren, Ground based and satellite observations of cloud fields in the Netherlands, *Mon. Wea. Rev.*, *124*(9), 1914–1923, 1996.

Grell, G. A., J. Dudhia, and D. R. Stauffer, A Description of the Fifth-Generation Penn State/NCAR Mesoscale Model (MM5), Tech. Rep. NCAR/TN-398+STR, National Center for Atmospheric Research (NCAR), Boulder (Co), USA, 1995.

Hanna, S. R., and R. Yang, Evaluation of Mesoscale Models' Simulations of Near-Surface Winds, Temperature Gradients, and Mixing Depths, *J. Appl. Meteorol.*, *40*, 1095–1104, 2001.

Hogrefe, C., et al., Evaluating the performance of regional-scale photochemical modelling systems: Part I — meteorological predictions, *Atmos. Environ.*, *35*, 4159–4174, 2001.

Holtslag, A. A. M., and B. A. Boville, Local vs nonlocal boundary-layer diffusion in a global model, *J. Climate*, *6*, 1825–1842, 1993.

Hong, S. Y., and H. L. Pan, Nonlocal boundary layer vertical diffusion in a medium-range forecast model, *Mon. Wea. Rev.*, *124*, 2322–2339, 1996.

Janjić, Z. I., The step-mountain coordinate model: Physical package, *Mon. Wea. Rev.*, *118*, 1429–1443, 1990.

Janjić, Z. I., The Step-Mountain Eta Coordinate Model: Further Developmenents of the Convection, Viscous Sublayer, and Turbulence Closure Schemes, *Mon. Wea. Rev.*, *122*, 927–945, 1994.

Oncley, S. P., and J. Dudhia, Evaluation of surface fluxes from MM5 using observations, *Mon. Wea. Rev.*, *123*, 3344–3357, 1995.

Pagowski, M., and G. W. K. Moore, A numerical study of an extrem cold-air outbreak over labrador sea: sea ice, air-sea interaction, and development of polar lows, *Mon. Wea. Rev.*, *129*, 47–72, 2001.

Raschke, E., and co-authors, BALTEX (Baltic Sea Experiment): A European Contribution to investigate the energy and water cycle over a large drainage basin., *Bull. Amer. Met. Soc.*, *82*(11), 2389–2413, 2001.

Seaman, N. L., Meteorological modelling for air-quality assessment, *Atmos. Environ.*, *34*, 2231–2259, 2000.

Seaman, N. L., F. L. Ludwig, E. G. Donall, T. T. Warner, and C. M. Bhumralkar, Numerical studies of urban planetary boundary-layer structure under realistic syniptic conditions, *J. Appl. Meteorol.*, *28*, 760–781, 1989.

Seibert, P., F. Beyrich, S. E. Gryning, S. Joffre, A. Rasmussen, and P. Tercier, Review and intercomparison of operational methods for the determination of the mixing height, *Atmos. Environ.*, *34*, 1001–1027, 2000.

Shafran, P. C., N. L. Seaman, and G. A. Gayno, Evalution of Numerical Predictions of Boundary Layer Structure during the Lake Michigan Ozone Study, *J. Appl. Meteorol.*, *39*, 412–426, 2000.

Stull, R. B., *An Introduction to Boundary Layer Meteorology*. Kluwer Academic Publishers, Dordrecht, The Netherlands, 1997 edn., 1988.

Troen, I., and L. Mahrt, A simple model of the atmospheric boundary layer; sensitivity to surface evaporation, *Bound.-Layer Meteo.*, *37*, 129–148, 1986.

Warner, T. T., and R. S. Sheu, Multiscale Local Forcing of the Arabian Desert Daytime Boundary Layer, and Implications for the Dispersion of Surface-Released Contamainants, *J. Appl. Meteorol.*, *39*, 686–707, 2000.

Zamora, R. J., J. W. Bao, A. B. White, and M. Trainer, An evaluation of MM5 surface fluxes and mixing depths during the Nasville southern oxidant studies, in *14th Symposium on Boundary Layer and Turbulence*, Aspen, USA. American Meteorlogical Society, 2000.

Zhang, D., and R. A. Anthes, A High-Resolution Model of the Planetary Boundary Layer—Sensitivity Tests and Comparisons with SESAME-79 Data, *J. Appl. Meteorol.*, *21*, 1594–1609, 1982.

Zhong, S., J. D. Fast, and X. Bian, The Influence of Boundary Layer and Surface Parameterizations on Simulations of Terrain-Induced Flows in the Salt Lake Valley, in *The Eleventh PSU/NCAR Mesoscale User's Workshop*, pp. 118–121, Boulder (CO), USA. 2001.

Received _____

This manuscript was prepared with AGU's LaTeX macros v4, with the extension package 'AGU++' by P. W. Daly, version ? from ?.

## Figure Captions

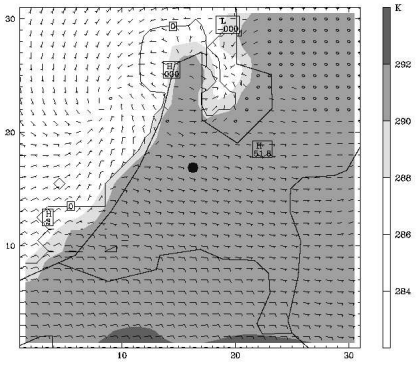


**Figure 1.** *The predicted wind-field and ground temperatures for most of The Netherlands by mesoscale modelling-system MM5 using* MRF*, during the synoptic situation of day 123 at 12* UTC*, where a sea-breeze can clearly be noticed along the north-west coastline. The dot (•) indicates the location of the observational tower of Cabauw.*

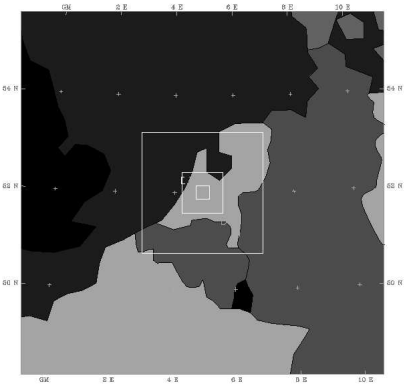

**Figure 2.** *Configuration of the three — two-way nested — domains where the Cabauw-site is centered inside the smallest domain and the coarse domain is represented by the figure's border.*

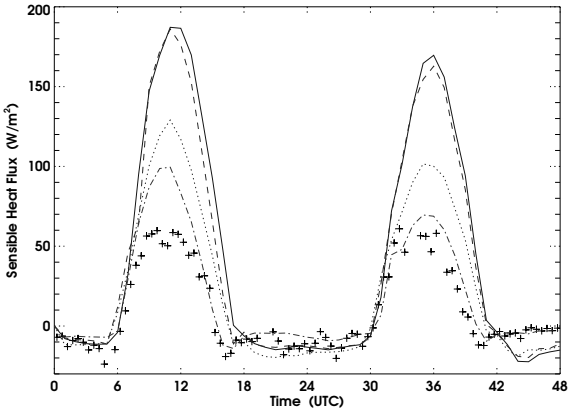


**Figure 3.** *Time evolution of the observed and simulated sensible heat flux at Cabauw, The Netherlands, for day 122 and 123. The Cabauw surface-observations plotted at 30-min time intervals are represented by a cross. The simulation results plotted at 1-h time intervals are represented by the following lines:* MRF *(solid),* BLA *(dashed),* Eta *(dotted),* BRT *(dash-dotted).*

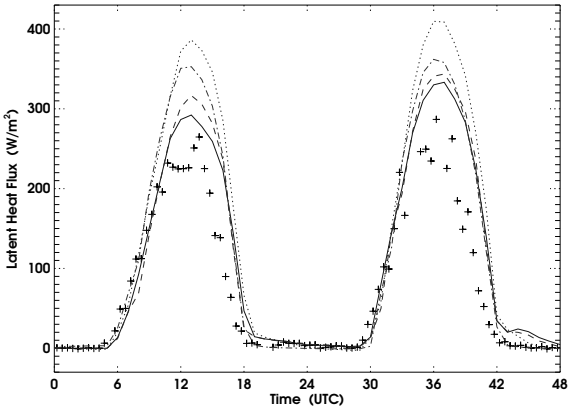


**Figure 4.** *Same as Fig. 3, but for the latent heat flux.*

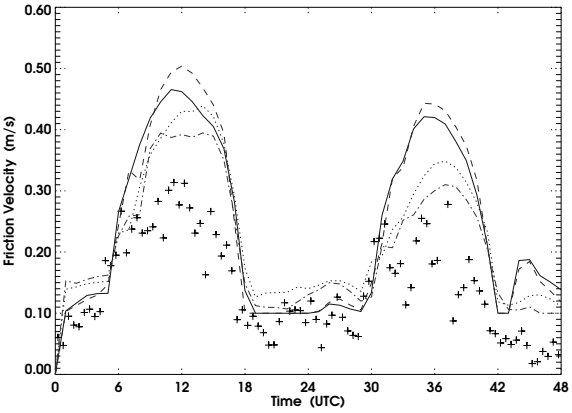


**Figure 5.** *Same as Fig. 3, but for the friction velocity.*

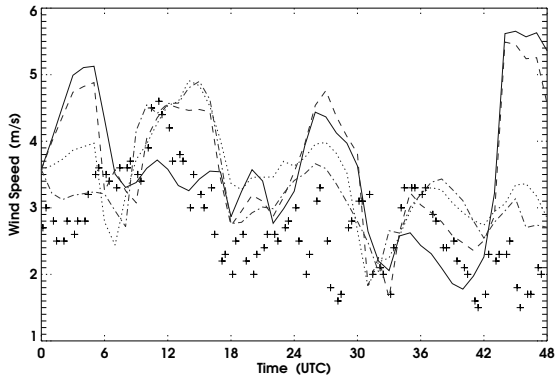


**Figure 6.** *Same as Fig. 3, but for the near-surface wind-speed at* 0.6 *m* AGL *compared to the Cabauw tower-observations at* 10 *m* AGL.

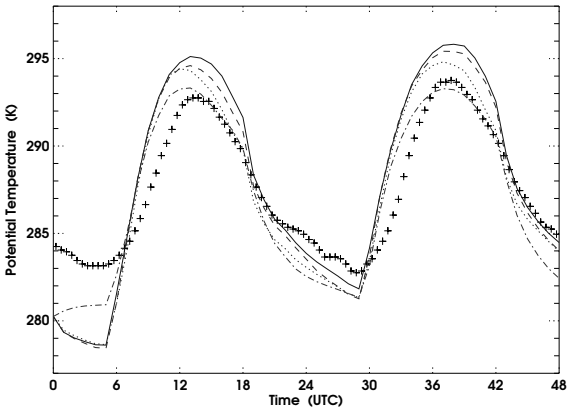


**Figure 7.** *Same as Fig. 3, but for the ground temperature.*

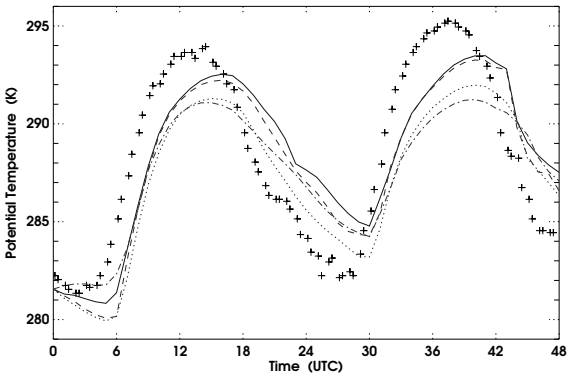


**Figure 8.** *Same as Fig. 3, but for the near-surface potential temperature at* 0.6 *m* AGL *compared to the Cabauw tower-observations at* 0.6 *m* AGL.

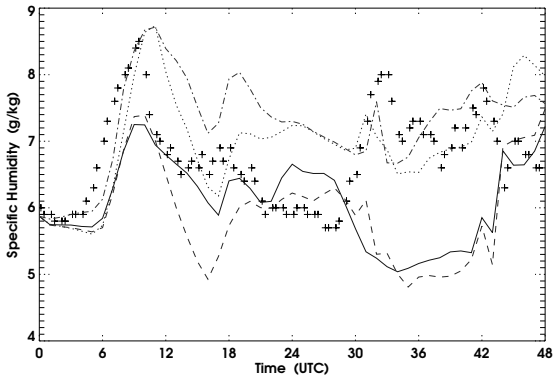


**Figure 9.** *Same as Fig. 3, but for the near-surface specific humidity at* 0.6 *m* AGL *compared to the Cabauw tower-observations at* 0.6 *m* AGL.

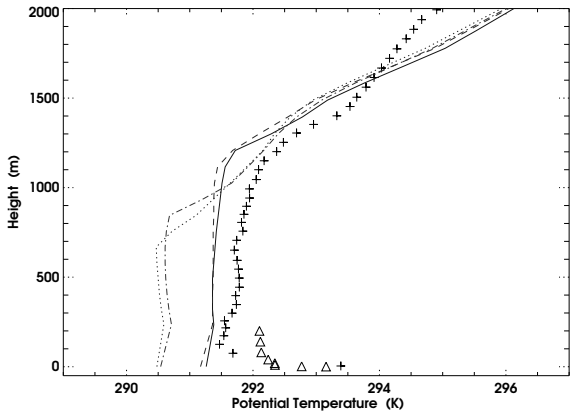


**Figure 10.** *The observed and simulated vertical profiles of potential temperature at 12* UTC *for day 122. The* TEBEX*-radiosounding at De Bilt and the Cabauw-tower observations are represented by a cross and triangle, respectively. The simulation results are represented by the following lines:* MRF *(solid),* BLA *(dashed),* Eta *(dotted),* BRT *(dash-dotted).*

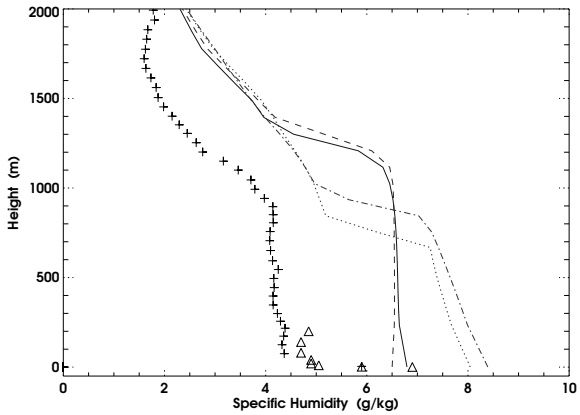


**Figure 11.** *Same as Fig. 10, but for the specific humidity.*

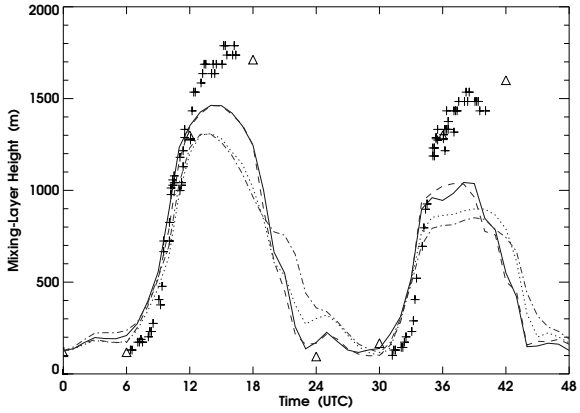


**Figure 12.** *The observed and simulated mixing-layer heights. The remote-sensing measurements of Cabauw, plotted at 15-min time intervals, and the* TEBEX*-radiosoundings at De Bilt are represented by a cross and a triangle, respectively. The simulation results are represented by the following lines:* MRF *(solid),* BLA *(dashed),* Eta *(dotted),* BRT *(dash-dotted).*

## Tables

| **Domain** | **1** | **2** | **3** | **4** |
|---|---|---|---|---|
| **Basic Model-Configurations** [1] | | | | |
| **Moisture Scheme**[2] (IMPHYS) | simple ice | simple ice | simple ice | simple ice |
| **Cumulus Scheme** (ICUPA) | Kain-Fritsch | Kain-Fritsch | none | none |
| **Radiation Scheme** [3] (FRAD) | cloud | cloud | cloud | cloud |
| **Shallow Convection** (ISHALLO) | none | none | none | none |
| FDDA & **Nudging** | no | no | no | no |

**Table 1.** *Overview of the most relevant physical options chosen in the MM5 modelling-system, applying to all numerical simulations implemented in this study.*

| **Experiment** | **1** | **2** | **3** | **4** | **5** | **6** |
|---|---|---|---|---|---|---|
| **Name** | *Default* | *Sin-up* | **Control** | *Roughness Length* | *Land-Use* | *Soil-Model* |
| **Simulation Settings** [4] | | | | | | |
| **PBL-scheme** (IBLTYP) | MRF, Eta | MRF, Eta | all 4 schemes | MRF | MRF | MRF |
| **Spin-up Time** $[h]$ | 0 | 24 | 0 | 0 | 0 | 0 |
| **Moisture Availability** [%] | 30 | 30 | 60 | 60 | 60 | 60 |
| **Roughness Length** $[cm]$ | 15 | 15 | 15 | 5 | 12 | 15 |
| **Land-Use Category** [5] $[no.]$ | 2 | 2 | 2 | 2 | 7 | 2 |
| **Soil-Model** (ISOIL) | 5L-LSM | 5L-LSM | 5L-LSM, Slab | 5L-LSM | 5L-LSM | 5L-LSM, OSU-LSM |
| **Global Analysis Data** | ECMWF | ECMWF | ECMWF | ECMWF | ECMWF | NCEP |

**Table 2.** *Specific settings of all numerical experiments implemented for this study.*